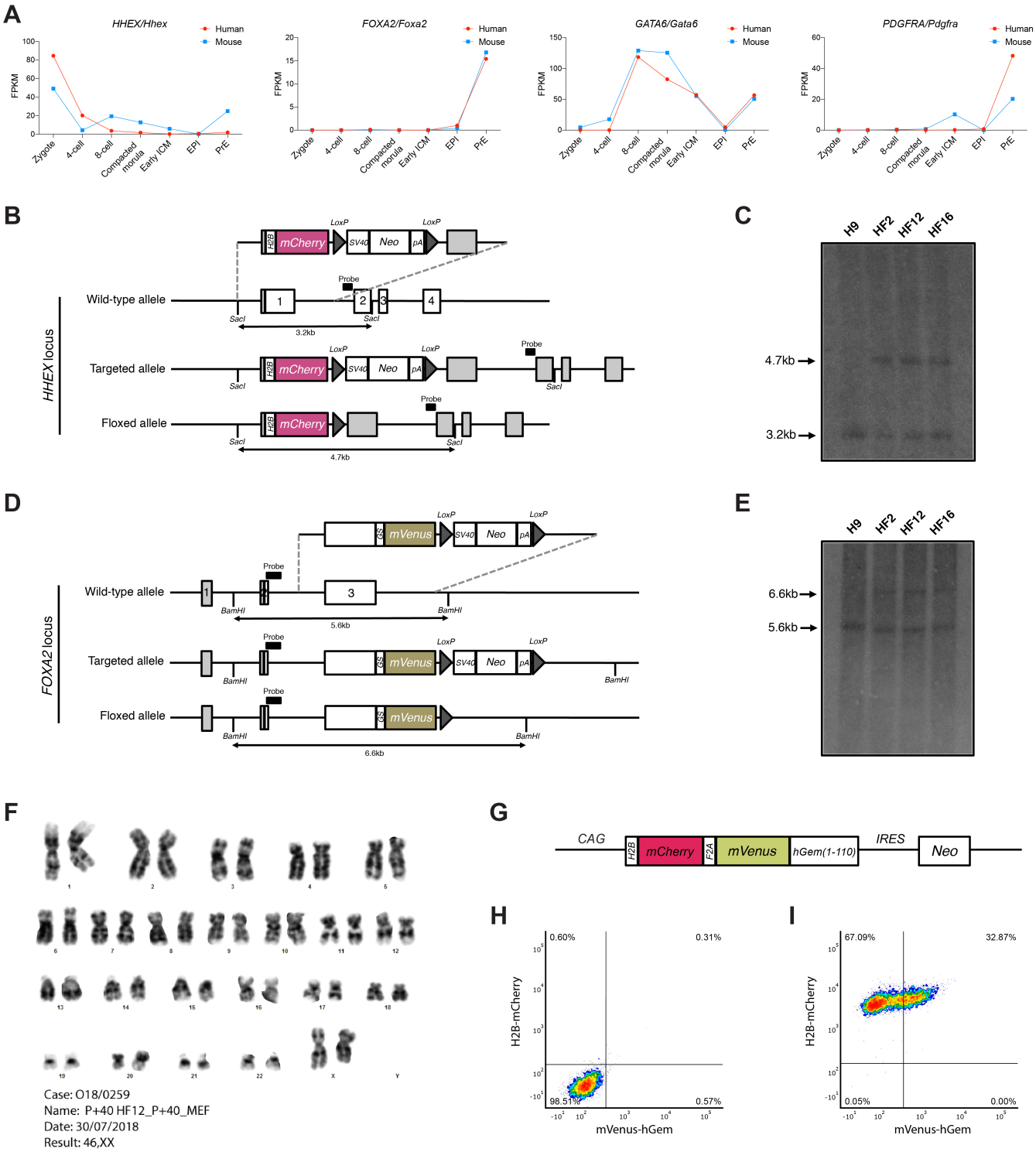

Figure S1: Description of reporter cell lines. (A) Expression of endodermal markers in the human blastocyst across early developmental stages from single-cell sequencing data **(Stirparo et al., 2018)**. (B, D) Schematics depicting the *HHEX-mCherry* and *FOXA2*-mVenus (H9-HF) reporter generated by CRISPR/Cas9-mediated homologous recombination. (C, E) Southern blot of the H9-HF reporter cell line showing the wild type gene sizes and the labelled targeted fragments. (F) HF12 was karyotyped, where the chromosome count was 46. (G) Schematic depicting the *H2B-mCherry-F2A-mVenus-hGem(1-110)* (H9-G2M) reporter driven by the *CAG* promoter generated by random integration. (H) Representative flow cytometry density plot showing gating strategy for wild type H9 hESCs for H2B-mCherry and mVenus-hGem expression. (I) Flow cytometry analysis confirming the H9-G2M reporter in primed media (KSR/FGF), as shown by all cells marked by H2B-mCherry, with a subset of proliferating cells expressing mVenus-hGem.

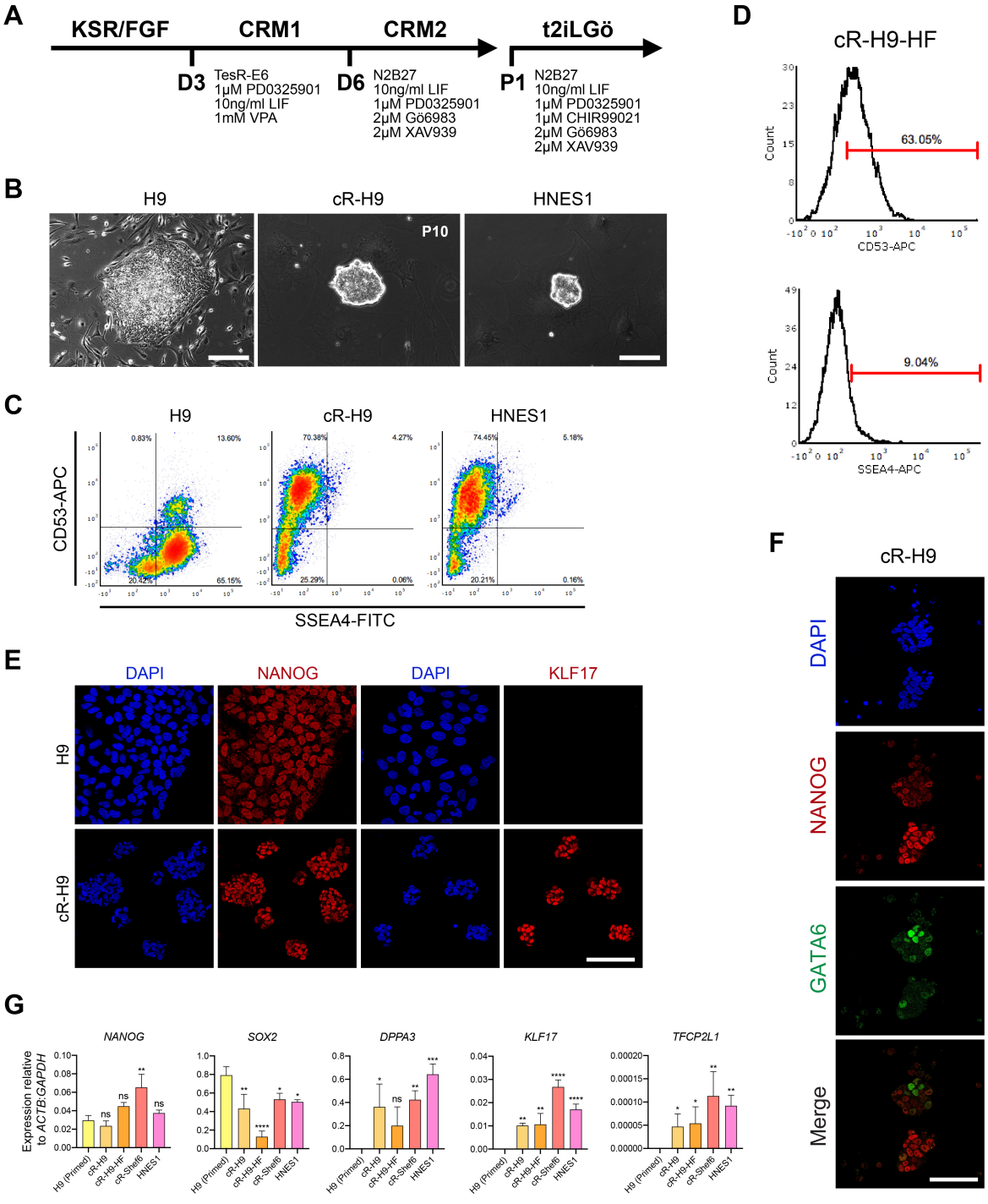

Figure S2: Chemical resetting of primed hESCs to the naïve state. (A) Schematic of the chemical resetting protocol including media compositions. (B) Brightfield images of primed H9 compared to cR-H9 and the embryo-derived HNES1. (C) Flow cytometry analysis of primed H9, cR-H9 and HNES1 with staining for primed-specific SSEA4 and naïve-specific CD53. Lower left quadrant indicates gating based on the negative control. (D) As cR-H9-HF could not be stained for SSEA4-FITC, a SSEA4-APC antibody was used instead. Histograms show fluorescence distribution of SSEA4-APC and CD53-APC expression in cR-H9-HF. cR-H9-G2M could not be analysed by flow cytometry due to problems with compensation. Horizontal bar indicates gating against the negative control with no antibody. (E) Immunostaining of primed H9 and cR-H9 for the pluripotency-associated marker NANOG and the naïve-specific marker KLF17, including DAPI, and imaged by confocal microscopy. (F) Immunostaining of cR-H9 for the indicated markers, including DAPI, and imaged by confocal microscopy. (G) qRT-PCR for pluripotency and naïve marker expression across various cell lines relative to *ACTB* and *GAPDH*. Scale bars: 100μm and 50μm in B (left to right); 25μm in E, F.

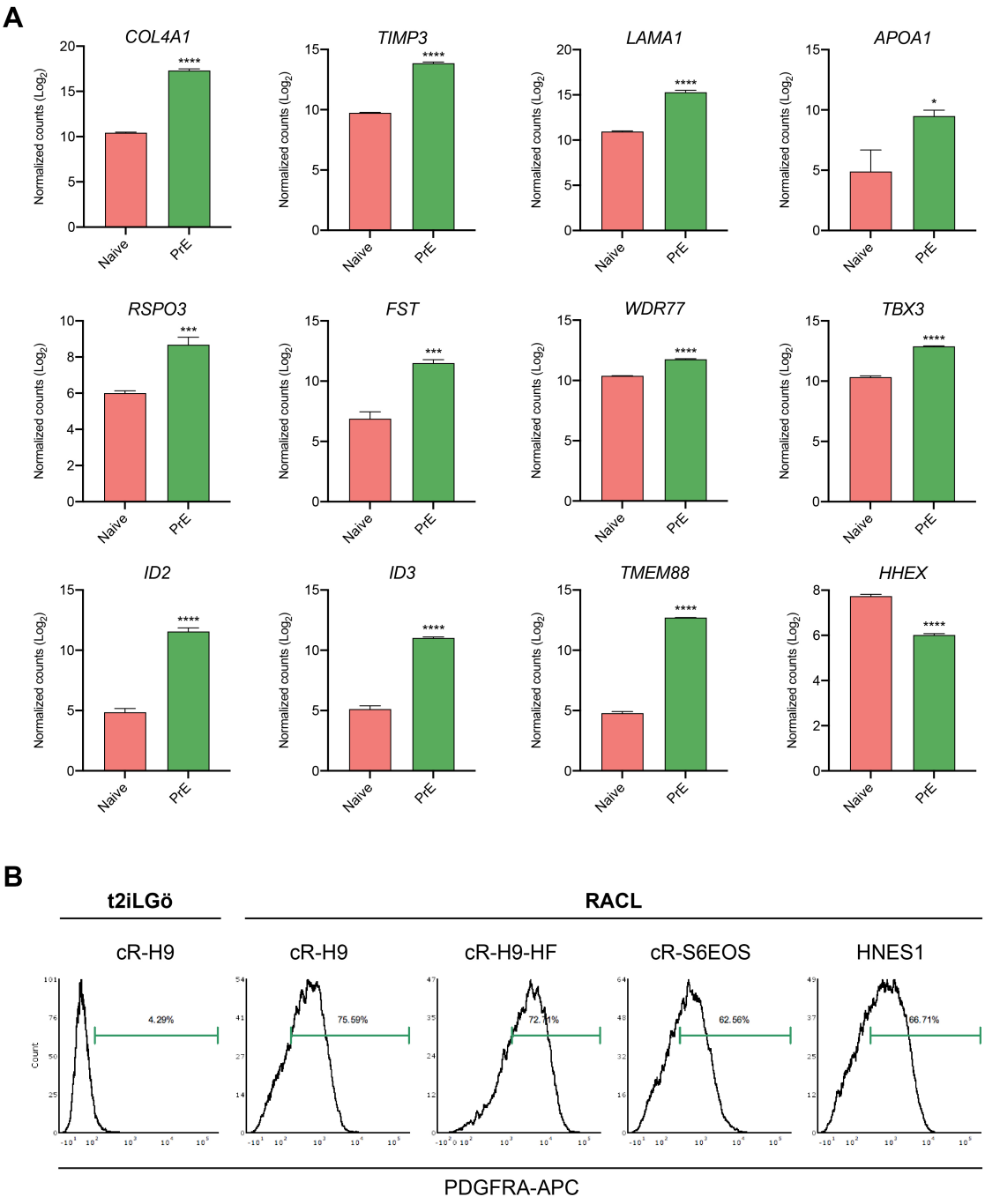

Figure S3: Human blastocyst endoderm marker expression in *in* vitro cell types. (A) Expression of indicated PrE markers **(Yan et al., 2013; Blakeley et al., 2015)** in RNA-sequencing data from naïve hESCs in t2iLGö and PrE. (B) Flow cytometry histograms for PDGFRA expression after PrE differentiation across different cell lines. Horizontal bar indicates gating based on the negative control with no antibody. Representative of 5 differentiations.

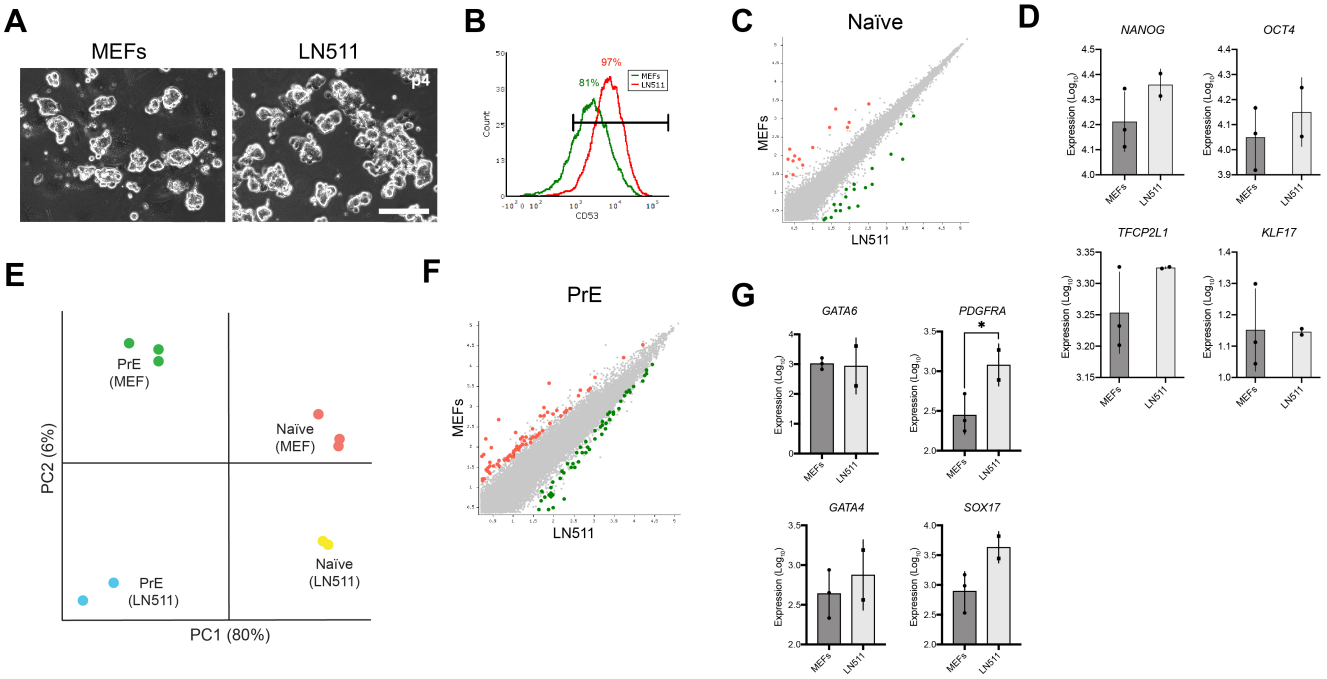

Figure S4: LN511 supports naïve hESCs and PrE differentiation in a feeder-free system. (A) Brightfield images of cR-H9 cultured on MEFs and LN511 for 4 passages in t2iLGö. (B) Histograms representing fluorescence for CD53 expression in cR-H9 maintained on either MEFs or LN511. Horizontal bar indicates gating against the negative control with no antibody. (C, F) Pairwise comparison of gene expression of microarray data for (C) naïve hESCs cultured on LN511 vs MEFs and (F) PrE differentiated on LN511 vs MEFs (fold change (FC) ≤ 1.5, FDR threshold ≤ 0.05). (D, G) Total expression of (D) pluripotency markers in naïve hESCs maintained on MEFs or LN511, and (G) PrE-specific markers in PrE differentiated on MEFs or LN511 based on microarray datasets. *n*=3 biological replicates for naïve cR-H9 on MEFs, *n*=2 from cR-H9 and *n*=1 from HNES1 differentiated to PrE on MEFs; *n*=2 biological replicates for cR-H9 cultured and differentiated on LN511 (E) PCA of microarray datasets from cR-H9 maintained on either LN511 or MEFs and differentiated to PrE on each substrate, as well as HNES1 differentiated to PrE on MEFs. *n* values as above. Scale bars: 100μm in A.

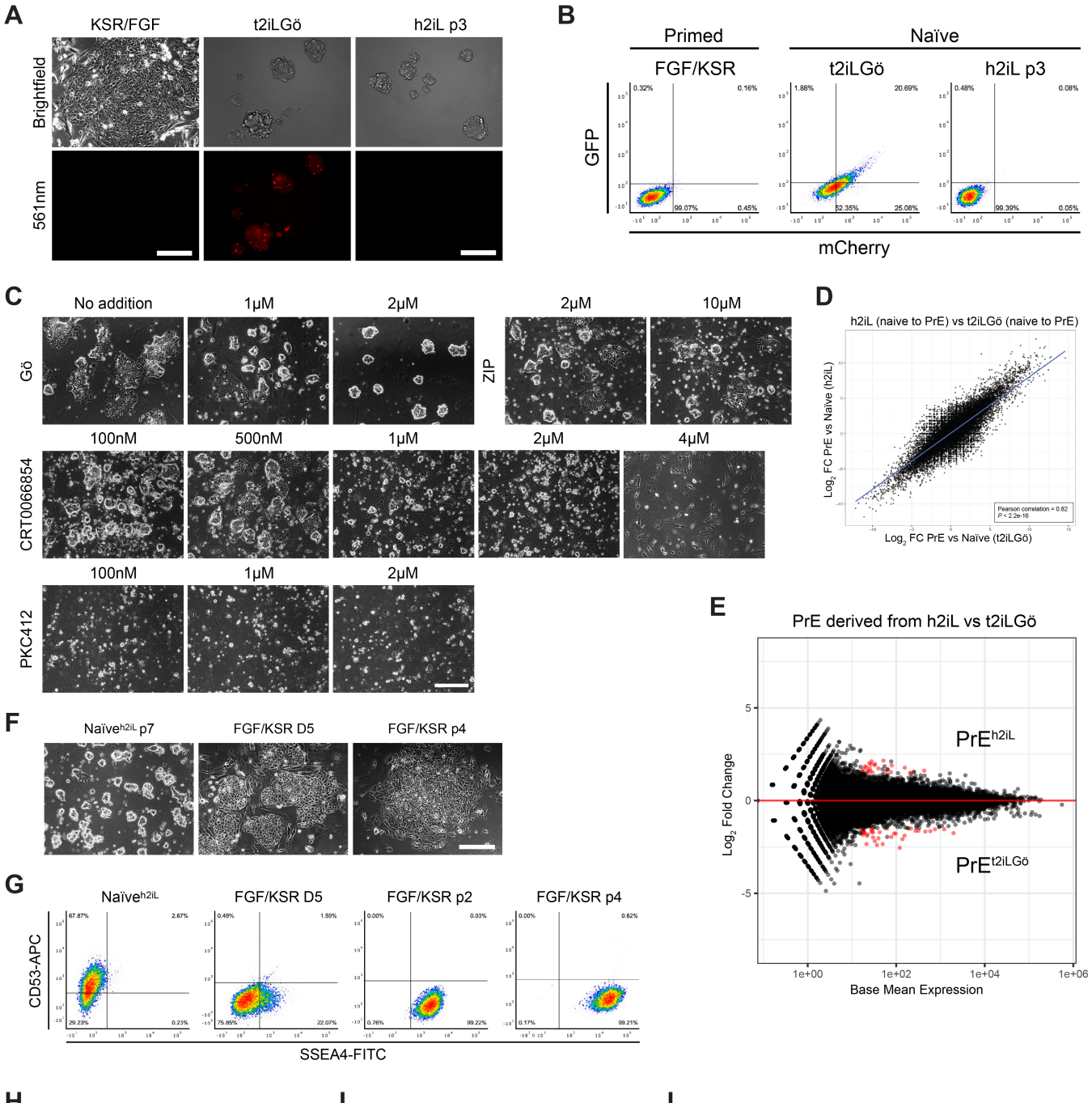

Figure S5: Assessment of signalling inhibitors in naïve pluripotent and differentiating culture. (A) Live primed H9 in KSR/FGF, cR-H9 in t2iLGö and cR-H9 in h2iL imaged by fluorescent microscopy. Bright red aggregates can be seen in cR-H9 cultured in t2iLGö. (B) Representative density plots of primed H9 ESCs in KSR/FGF, cR-H9 in t2iLGö and h2iL, showing autofluorescence produced by Gö in the t2iLGö condition. Lower left quadrant indicates gating based on the negative control. (C) Brightfield images of cR-H9 cultured in t2iL supplemented with different aPKC inhibitors at the indicated concentrations. (D) Pearson correlation dot plot showing $\log_2$ FC in global gene expression between naïve and PrE samples in t2iLGö and h2iL. (E) MA-plot representing differential expression analysis of PrE differentiated from naïve hESCs maintained in h2iL vs t2iLGö (1.5 $\log_2$ FC, $p<0.05$), where red dots indicate genes that are differentially expressed (n=25 genes in PrE^{h2iL} and n=35 genes in $PrE^{t2iLGö}$). (F-G) Conversion of $naïve^{h2iL}$ cells back to primed pluripotency. cR-H9 were cultured in h2iL for 7 passages and then placed back into primed culture (FGF/KSR) for 4 passages. (F) Brightfield images of cR-H9 in initial naïve h2iL culture and 4 passages after transfer to primed medium. (G) Flow cytometry density plots of the naïve-to-primed transition for CD53 and SSEA4 expression. Quadrants based on gating against the negative control with no antibody. (H-I) Flow cytometry histograms for naïve hESCs cultured in N2B27 supplemented with 10ng/mL LIF, 1μM CHIR, as well as various concentrations of (H) PD17, (I) the VEGFR inhibitor CBO-P11, and (J) the EGFR inhibitor PD153053. Horizontal bar indicates gating against the negative control with no antibody. Scale bars: 100μm and 50μm in A (left to right); 50μm in C; 100μm in F.

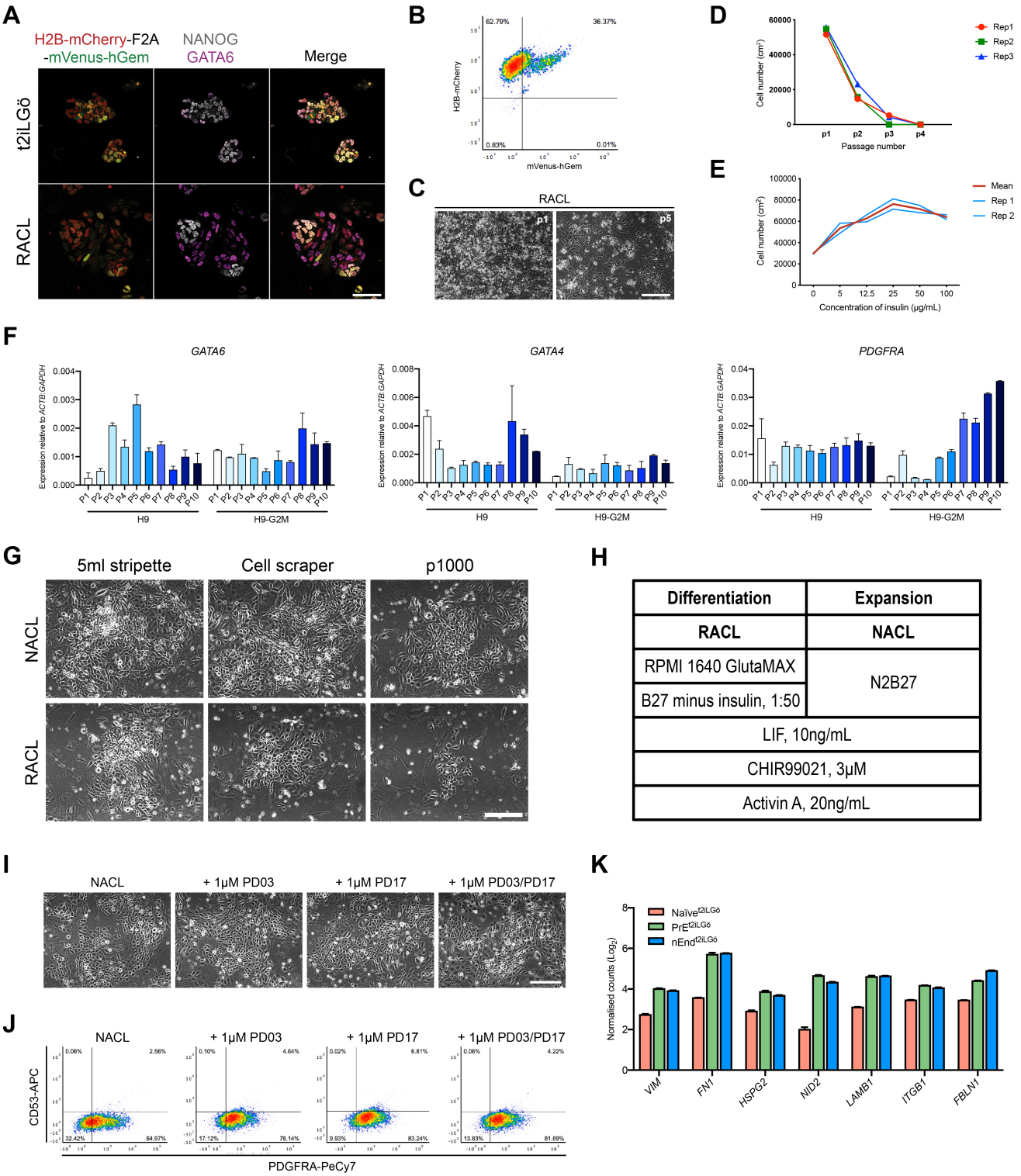

Figure S6: Expansion of naïve extra-embryonic endoderm is supported by insulin. (A) cR-H9-G2M naïve^{h2iL} hESCs and subsequent differentiation to PrE imaged by confocal microscopy. H2B-mCherry expression marks all cells, while mVenus-hGem specifies cells in G2/M. (B) Dot plot based on flow cytometry analysis of H2B-mCherry and mVenus-hGem expression in H9-G2M passaged nEnd. (C) Brightfield images of naïve cR-H9 differentiated to PrE in RACL and passaged in RACL medium. (D) Cell numbers of cR-H9 differentiated and passaged in RACL, where cells were plated at a 1:1 ratio at each passage. (E) Cell numbers of cR-H9 PrE cultured in titrated concentrations of insulin (*n*=2 biological replicates, with the mean shown in red). (F) qRT-PCR showing relative expression of PrE markers during expansion of cR-H9 and cR-H9-G2M nEnd in NACL. Error bars indicate ± s.d. of technical replicates (*n*=1 biological replicate for each cell line shown). (G) Brightfield images of cR-H9 PrE expansion in RACL or NACL, using three different passaging techniques. Representative of 3 different cell lines. (H) Overview of culture media composition in PrE differentiation and expansion. (I-J) nEnd expansion does not require FGF/ERK signalling. HNES1 nEnd^{t2iLGö} (passage 8) was passaged to NACL supplemented with 1μM PD032501, 1μM PD173074 or both for 5 days. (I) Brightfield microscopy showing nEnd morphology, and (J) expression of cell surface markers PDGFRA and CD53 in all three conditions by flow cytometry analysis. (K) Comparative expression of BM components in naïve^{t2iLGö} cells compared to PrE and nEnd derived from these, based on RNA sequencing data. Scale bars: 25μm in A; 100μm in C, G, and I.

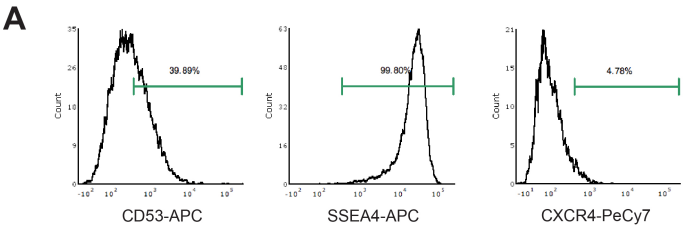

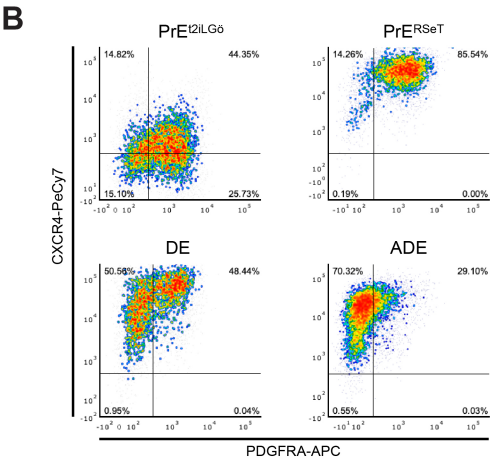

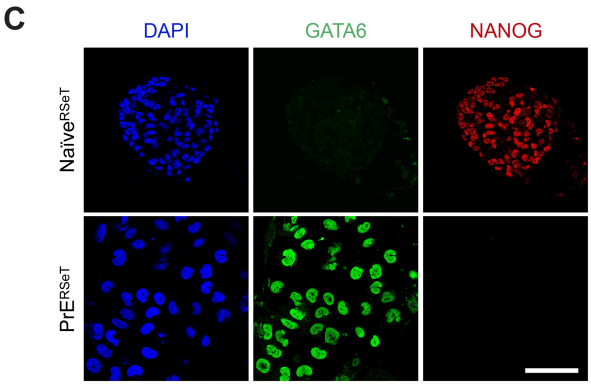

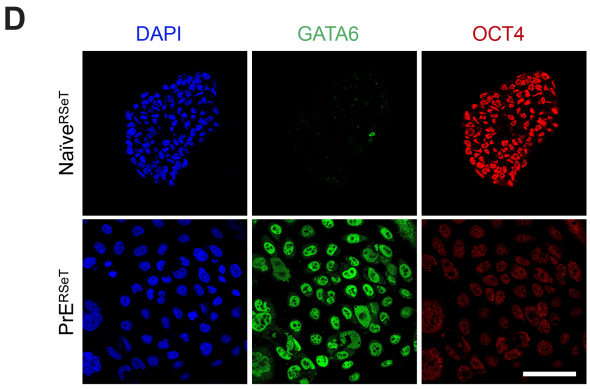

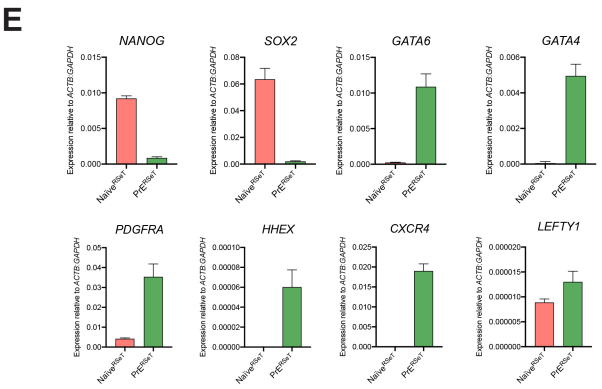

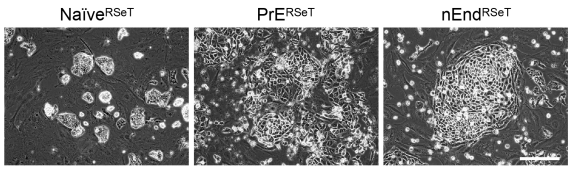

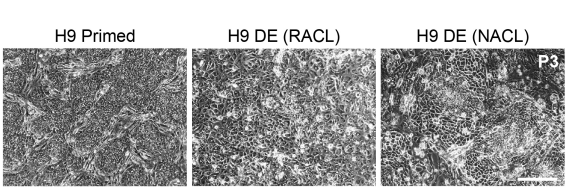

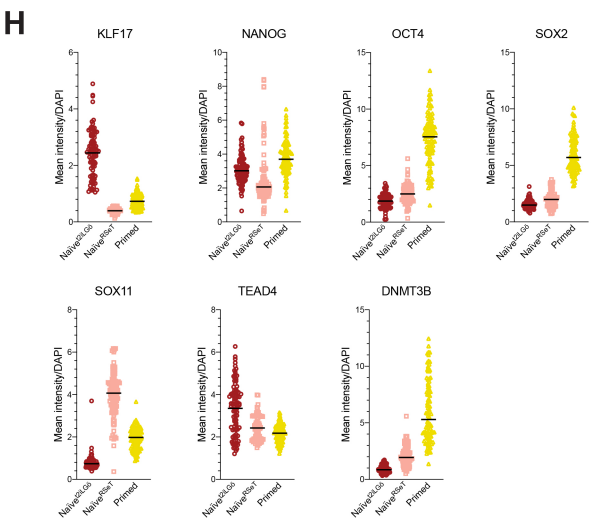

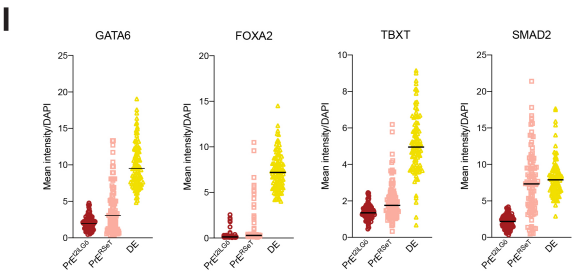

Figure S7: Derivation and differentiation of endoderm from RSeT naïve ESCs. (A) Histograms depicting expression of indicated surface markers in ESCs maintained in RSeT medium. Horizontal bar indicates gating against the negative control with no antibody. (B) Density plot for flow cytometry analysis of naïve^{RSeT}-derived PrE for CXCR4 and PDGFRA compared to PrE from naïve^{t2iLGö} cells, as well as DE and ADE from primed hESCs. (C-D) Immunostaining of naïve^{RSeT} and PrE derived from these for (D) NANOG and GATA6 and (E) OCT4 and GATA6, with inclusion of DAPI. (E) qRT-PCR showing relative expression of indicated pluripotency and endoderm markers in naïve^{RSeT} hESCs and subsequent endoderm. (F) Brightfield images of naïve^{RSeT} ESCs differentiated to endoderm in RACL for 7 days and expansion in NACL. (G) Brightfield images of primed H9 hESCs differentiated to DE in RACL for 5 days and attempt at expansion in NACL. (H-I) Single-cell analysis of (H) ESCs (naïve^{t2iLGö}, naïve^{RSeT}, primed) and (I) endoderm differentiation from these ESCs (PrE^{t2iLGö}, PrE^{RSeT}, DE) by quantitative immunofluorescence for indicated markers normalised to DAPI nuclear stain (*n*=100 cells). Scale bars: 50μm for C, D; 100μm for F, G.

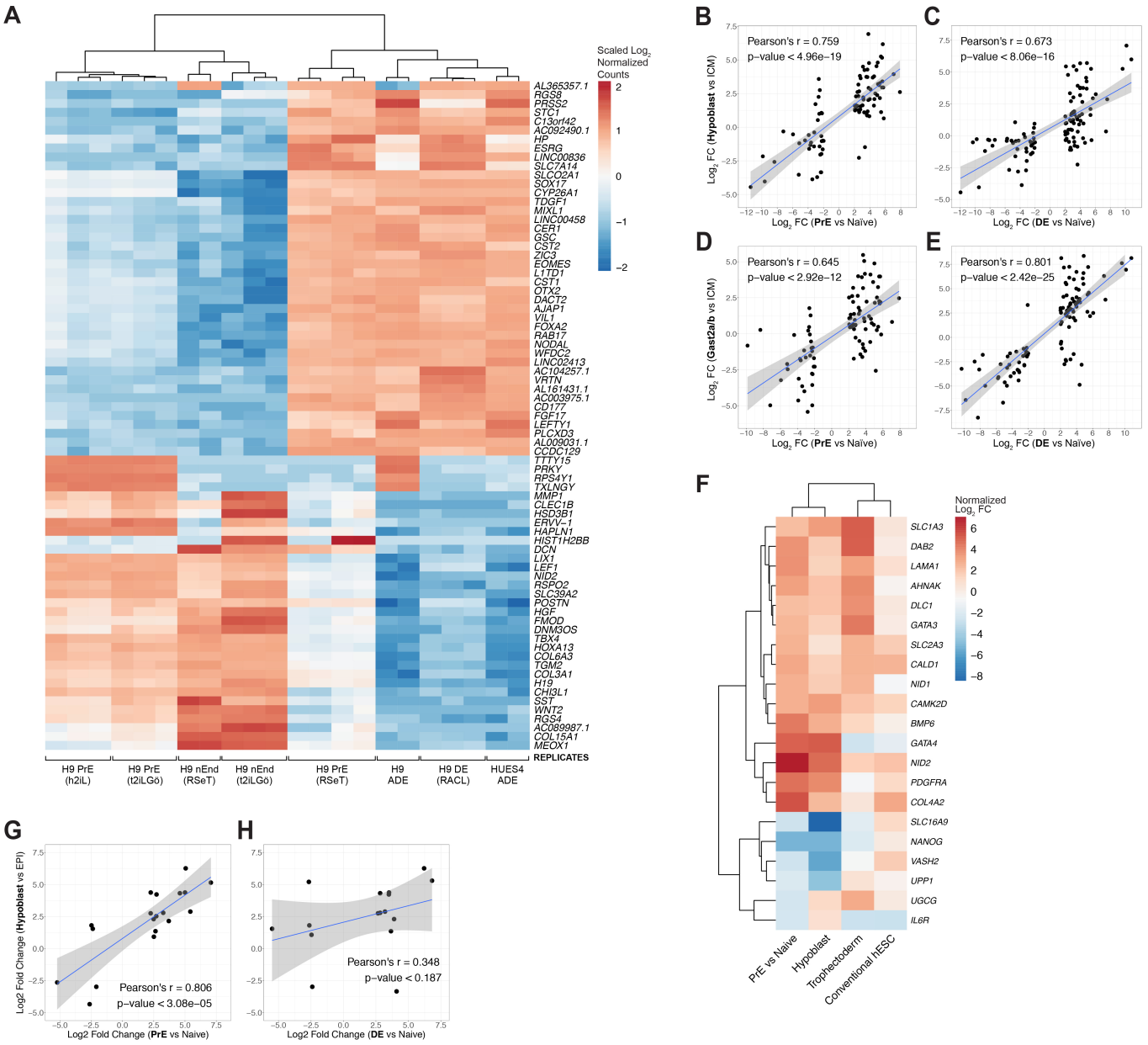

Figure S8: Analysis of *in vitro* transcriptomes and comparison to single-cell *in vivo* datasets derived from human and cynomolgus monkey.

(A) Representation of top 70 most variable genes across all endodermal cell types based on whole-transcriptome analysis of *invitro* cultures. (B-E) Pearson correlation of $\log_2$ FC of common genes between cynomolgus monkey **(Nakamura et al., 2016)** *invivo* and human *invitro* cell types for (B) hypoblast vs ICM and PrE/nEnd vs naïve ESCs (*n*=92 genes), (C) hypoblast vs ICM and DE vs naïve ESCs (*n*=110 genes), (D) Gast2a/b vs ICM and PrE/nEnd vs naïve ESCs (*n*=93 genes), and (E) Gast2a/b vs ICM and DE vs naïve ESCs (*n*=108 genes). (F) Comparative analysis of $\log_2$ FC of common genes (*n*=19) between human early cell types vs EPI **(Yan et al., 2013; Blakeley et al., 2015)** and human *invitro* PrE/nEnd vs naïve cells. (G-H) Pearson correlation of $\log_2$ FC of common genes between human early cell types vs EPI **(Yan et al., 2013; Blakeley et al., 2015)** and human *invitro*; (G) PrE/nEnd vs naïve ESCs (*n*=19 genes), and (H) DE vs naïve ESCs (*n*=16 genes).

Table S1. A**:** Differentially upregulated genes in PrE compared to DE; B: Differentially downregulated genes in PrE compared to DE; C: Uniquely differentially upregulated genes in PrE compared to DE; D: Uniquely differentially downregulated genes in PrE compared to DE

Click here to Download Table S1

Table S2. A: Overexpressed genes in naive hESCs cultured on LN511 vs MEFs; B: Underexpressed genes in naive hESCs cultured on LN511 vs MEFs; C: Overexpressed genes in PrE differentiated on LN511 vs MEFs; D: Underexpressed genes in PrE differentiated on LN511 vs MEFs

Click here to Download Table S2

Table S3. A: Overexpressed genes in naive hESCs cultured in h2iL vs t2iLGö; B: Underexpressed genes in naive hESCs cultured in h2iL vs t2iLGö; C: Overexpressed genes in PrE differentiated from h2iL vs t2iLGö; D: Underexpressed genes in PrE differentiated from h2iL vs t2iLGö

Click here to Download Table S3

Table S4. A: EPI and PrE markers (Stirparo *et al*., 2018); B: Naive and primed markers (Messner *et al*., 2019)

Click here to Download Table S4

Table S5: Antibodies

Antibody	Vendor	Catalogue number	Concentration
CD53-APC	Miltenyi Biotec	130101795	1:50
CXCR4-PeCy7	BD Bioscience	560669	1:100
DAPI	Thermo Fisher	D1306	1:5000
PDGFRa-APC	BD Bioscience	562798	1:100
SSEA4-647	Molecular Probes	SSEA421	1:1000
SSEA4-FITC	BioLegend	330409	1:100
GATA4	Santa Cruz	sc1237	1:1000
GATA6	R&D	AF1700	1:500
KLF17	Sigma-Aldrich	hpa024629	1:1000
NANOG	Abcam	ab21624	1:1000

Table S6: qRT-PCR primers and probe pairs

Gene	Forward Primer	Reverse Primer	Probe
ACTB	ccaaccgccgagaagatga	ccagcggcgtacagggatag	64
BMP6	tttccaagacctgggatgg	gcattcatgtgtgcgttga	12
CXCR4	cctgcctggtattgtcatcc	gatggggatgattgtggtct	49
DPPA3	gggaaatcgaagatgagtgg	aggctccttgtttgttggtc	18
GAPDH	agccacatcgctcagacac	gcccaatacgaccaaatcc	60
GATA4	ggaagcccaagaacctgaat	gttgctggagttgctggaa	17
GATA6	gcgggctctacagcaagat	tggcacaggacaatccaag	30
GSC	cctccgcgaggagaaagt	cgttctccgactcctctgat	29
HHEX	gcggacggtgaacgacta	ggccgcctttccttttat	50
HNF4A	acaatcgtcaagcccctct	ccagcggcttgctagataac	9
KLF17	ctcctgctgctggtccttag	cagttgccacgtccagtg	64
LEFTY1	aaagaggttcagccagagctt	caccagcaggtgtgtgct	72
MIXL1	ggtaccccgacatccactt	gcctgttctggaaccatacct	32
NANOG	gggaaaaagccagaagtcg	ctttggggacaagctgga	52
NID2	cctgcagctacctgctacaa	gtgtcaggcttgaggtggag	2
OCT4	gcttcaagaacatgtgtaagctg	cacgagggtttctgctttg	69
PDGFRA	tgcctgacattgaccctgt	ccgtctcaatggcactctc	63
SOX2	ttaaaagttctagtggtacggtaggag	ttcgtcgcttggagactagc	4
TFCP2L1	cctggtccaccacacctatt	atggtcatctttggcctcac	2